HYPERSPECTRAL REMOTE SENSING OF OCEAN COLOR: A COMPARISON OF HYPERION WITH AVIRIS

Marcos J. Montes,[*] Bo-Cai Gao,[†] and Curtiss O. Davis[§]

1. Introduction

Remote sensing has the promise to be a useful tool for observing the processes that occur on many spatial and temporal scales in the coastal ocean. The fairly high spatial resolution (~2–30 m) of the current generation of hyperspectral imagers allows for much detailed study of these areas than can be performed with moderate-resolution multi-spectral sensors such as Sea-viewing Wide Field-of-View Sensor (SeaWiFS) and Moderate-Resolution Imaging Spectrometer (MODIS). The Hyperion sensor aboard the Earth Observing 1 Satellite (EO-1) serves as a testbed for hyperspectral imagers in space. We acquired Hyperion imagery of the region around the Looe Key on October 26, 2002. A portion of the Hyperion scene was also observed in 1996 with the Airborne Visible Infrared Imaging Spectrometer (AVIRIS). We address issues of atmospheric correction and calibration and compare R_{rs} values for the intersecting portions of the AVIRIS and the Hyperion imagery.

2. Atmospheric Correction

Over the past two decades, atmospheric correction algorithms for application to case 1 waters (i.e., clear, deep ocean waters) have been developed by Howard Gordon's research group at the University of Miami. The complexity of these algorithms has increased greatly with time; from the early single scattering algorithm used for Coastal Zone Color Scanner—CZCS (Gordon, 1978) to the present, more complete multiple scattering algorithm for SeaWiFS (Gordon and Wang, 1994). For the operational SeaWiFS algorithm, a simplified two-layer atmosphere system, i.e., aerosols being confined in the bottom boundary layer and atmospheric gaseous molecules being located in another layer above the aerosol layer, is assumed. An aerosol model and an aerosol optical depth are derived from channels located centered at 0.76 and 0.87 μm by assuming water-leaving radiances to be zero in that spectral range. A sophisticated lookup table procedure is used for the aerosol retrievals. The atmospheric path radiances in the visible are predicted based on the derived aerosol information. The difference between the measured radiances above the atmosphere-ocean system and the predicted path-radiance is the water-leaving radiance transmitted to the top of the atmosphere.

However, this approach does not work for some ocean environments, such as the shallow ocean environment in this study. Over a bright sand bottom, a turbid coastal environment, or a coccolithophore bloom the water-leaving radiances in the 0.66–0.87 μm range are typically not close to zero. In the former case, reflectance by bright ocean bottoms in optically shallow water causes much more water leaving radiance at these wavelengths than is measured in open oceans with similar water types. In the latter cases, this is due to scattering by suspended materials. Under these conditions, the channels in this spectral region have very limited use for the retrieval of information on atmospheric aerosols. The algorithms of Gordon (1997) and Fraser et al. (1997) derive aerosol information from channels in the 0.66–0.87 μm spectral range. These algorithms cannot be easily adapted for the retrieval of water-leaving radiances over coastal waters. In view of this situation, we have designed a different retrieving algorithm that can use channels in longer wavelengths, in addition to these channels, to derive aerosol information.

Since the liquid water absorption increases rapidly as a function of wavelength, one can assume that the water leaving radiance is zero at long enough wavelengths, even in turbid waters or over bright, shallow bottoms. In this case, one can use two or more of the atmospheric transmission window regions near 0.865, 1.04, 1.24, 1.64, and/or 2.25 μm in order to determine the aerosol type and optical depth. Our Tafkaa aerosol lookup tables include all of those wavelengths, in addition to several in the visible and near-infrared (VNIR) portion of the spectrum. The tables were calculated with Ahmad and Fraser's (1982) radiative transfer code that includes all orders of scattering, and components of polarization. The lower boundary condition is a rough ocean surface with capillary wave distribution as described by Cox and Munk (1954), as well as the effects of foam. The tables were calculated at 14 wavelengths and 3 wind speeds. There are 10 aerosol optical depths, 5 overall aerosol models, each of which has 5

[*] U.S. Naval Research Laboratory, Code 7232, Washington, DC 20375; Marcos.Montes@NRL.Navy.mil
[†] U.S. Naval Research Laboratory, Code 7232, Washington, DC 20375
[§] U.S. Naval Research Laboratory, Code 7203, Washington, DC 20375

size distributions (i.e., relative humidities). The geometrical grids have 9 solar zenith angles (θ_0), 17 view zenith angles (θ), and 17 relative azimuth angles ($\Delta\phi$). The calculations were output at 9 sensor altitudes, and all the calculations assume a surface at sea-level. A thorough description of our algorithm may be found in Gao et al. (2000), and modifications are described in Montes et al. (2003).

3. Hyperion and AVIRIS

Some of the principal differences affecting coastal ocean data obtained with Hyperion and AVIRIS are listed in Table 1. Because it is airborne, AVIRIS can obtain data along many different possible paths, and the paths can have variable lengths. The satellite path of EO-1 and the small cross-track field of view limit the scenes obtained with Hyperion to particularly long and narrow (~7 km) swaths along the satellite's track. However, the very wide full-field of view for AVIRIS scenes can lead to solar glint or to cross-track differential specular reflection effects in a large fraction of an oceanic scene unless the ER-2 flight line is nearly into or out of the sun. Hyperion's much narrower field of view makes it relatively easier to avoid solar glint, especially with its ability to point off-nadir. On the other hand, the low signal-to-noise ratio (SNR) and the noisy data in the short-wave infrared (SWIR) make it difficult to use the SWIR bands for atmospheric correction as described in §2.

Table 1. Comparison of Design Features

	1996 AVIRIS	HYPERION
Sensor Design	Whisk broom, 4 spectrometers	Push broom, 2 spectrometers
Platform	Airborne ER-2 @ ~20km	EO-1 Satellite @ 705 km
Spectral Characteristics	224 bands, $\Delta\lambda$~10 nm, FWHM~10 nm, range: 0.375–2.50 μm	198 bands, $\Delta\lambda$ ~11 nm, FWHM ~11 nm; range: 0.43–2.4 μm
Typical GSD	~ 20 m from ER-2	~30 m from orbit
Full field of view	30° (~12 km at ER-2 altitude)	0.6° (~7 km from orbit)
SWIR Comments	Relatively high SNR	Relatively low SNR

4. Data and Processing

The AVIRIS and Hyperion data were obtained several years apart, with different orientation, in different seasons, and at different spatial scales. The AVIRIS data was obtained in a flight mostly along the Florida Keys, approximately from east to west. The Hyperion image, on the other hand, is mostly from north to south. While the solar zenith angles were fairly similar, the relative azimuth angles ($|\phi_0 - \phi|$) were quite different. For AVIRIS, ϕ changes at nadir assuming that the ER-2 is in level flight with no pitch or roll. In this case, ϕ takes on different values to the left and right of nadir, and typically $\phi_{left} = \alpha_h + 90°$ and $\phi_{right} = \alpha_h - 90°$ (where left and right refer to the plane in this case, and the view azimuth is measured from the surface to the sensor), so $\phi_{left} = 350°$ and $\phi_{right} = 170°$.

Table 2. Comparison of Data Collection Conditions

	AVIRIS	HYPERION	Comments
Data Set	f960323t01p02_r10a	EO1H0150432002299110KY	
Date (Gregorian / GMT)	1996 March 23	2002 October 26	Different Seasons
Time (24 hour GMT)	19:48	15:27	
Time (24 hour EST)	14:48	10:27	Afternoon vs. morning
Solar Zenith Angle θ_0	40°	45°	
Solar Azimuth Angle ϕ_0	240°	143°	Clockwise from N
View Zenith Angle θ	$0° < \theta < 15°$	27° (to the west of nadir)	Hyperion viewed off-nadir
View Azimuth Angle ϕ	See text	101°	Clockwise from N
Mean Heading α_h	260°	191°	Clockwise from N

Several features are easily recognizable in both images in Fig. 1, and the approximate borders of the region of overlapping data have been marked. The intersection of the images includes portions of No Name and Mayo Keys, Porpoise Key, a large part of Big Pine Key (the largest island in the imagery), all of Little Torch Key, Middle Torch Key, Ramrod Key, and portions of Big Torch and Summerland Keys. The pixels in the Hyperion image are markedly non-square due to the large view zenith angle of that data.

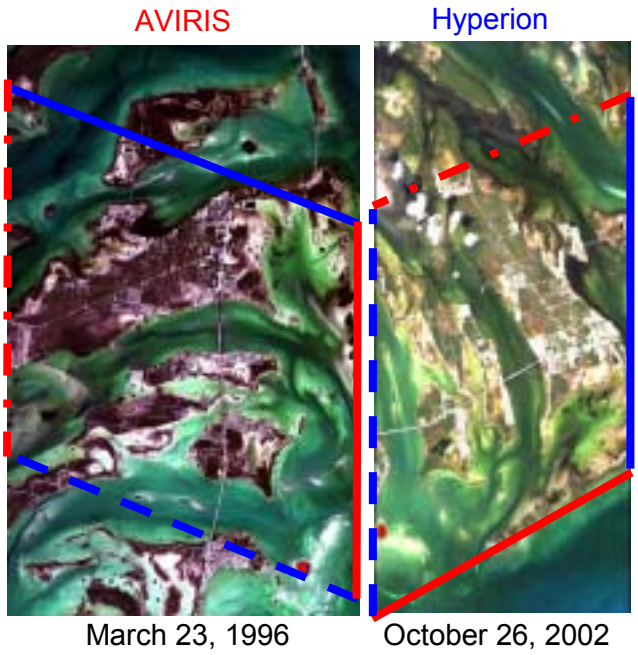

Figure 1. Images showing the approximate area of overlap between the AVIRIS and the Hyperion imagery. In this imagery, the eastern and western borders of the Hyperion image are the *solid* and *dashed* blue lines, respectively. Likewise, the southern and northern borders of the AVIRIS image are the *solid* and *dashed* red lines, respectively. The images are not to scale, and neither image has been geo-rectified. Due to the off-axis pointing of Hyperion, the cross-track ground sample distance (GSD) is ~ 34m, and its pixels are not square. Each image is a small portion of a much larger data set.

The AVIRIS data was processed using the standard Tafkaa processing chain. A land mask was created to mask the land in order to bring out the features in the water. Three, four, or five NIR/SWIR bands were used to determine the aerosol model using Tafkaa. Small effects arising from the cross-track viewing geometry and the changing along-track solar geometry were corrected for. While all areas were processed, we avoided analysis in areas with the "ghosts" that are present in the 1996 AVIRIS data (Montes, 2004) as these will give false aerosol retrievals.

The Hyperion processing was rather more involved as there are several artifacts that affect Hyperion data (Datt *et al.,* 2003; Goodenough *et al.,* 2003, Green *et al.,* 2003, and other articles in the TGARS *Special Issue on EO-1 Mission* 2003). We elected to use only the calibrated VNIR bands of the first spectrometer due to the low SNR in the SWIR spectrometer. It was necessary to apply a "flat-fielding" or "de-striping" process in order to remove (or reduce) along track striping in the imagery. We used our own custom written software implementing the process described in Kruse *et al*. (2003) in order to reduce the striping in the imagery. As we were using only the VNIR spectrometer, the only bands we could use in order to determine the aerosol parameters were the 0.750 μm and 0.865 μm bands. However, the presence of a bright, shallow bottom prevents us from using the 0.750 μm band for aerosol determination in large parts of the Hyperion image. Since we were not interested in correcting land or clouds, but we wanted to differentiate optically shallow water from much deeper water, we created a program to determine whether a pixel was land or water. All non-land, non-water pixels were called clouds. In general we can tolerate error in the land and cloud confusion since we were only concerned with water. A sub-class of shallow water pixels was determined from water pixels where $\rho^*_{obs}(0.79\ \mu m)/\rho^*_{obs}(0.75\ \mu m) > t$, where t=1.05 is a threshold determined from the data, $\rho^*_{obs}=\pi L/(\mu_0 E_0)$, $\mu_0 = \cos(\theta_0)$, and E_0 is the solar irradiance above the atmosphere. Standard pixel-to-pixel Tafkaa processing was performed on the data using the 0.750 μm and 0.865 μm bands to determine the aerosol model and optical depth in the non-shallow area. In the shallow areas, aerosol models and optical depths from nearby areas were used.

5. Results

The comparison of these data sets is problematic since they were obtained at such different times, and since there is no contemporaneous ground truth data for either date in the area where these images overlap. The tidal states are uncertain, so relative submerged depths are not known. However, tide charts show typical ranges of tides to be of order 0.40 m, so this uncertainty is not too large. The aerosol was retrieved using Tafkaa assuming there was no water leaving radiance at 0.865, 1.04, 1.24, and 1.64 μm for the AVIRIS data, and the retrieved aerosol optical depth at 0.55 μm τ_{550} = 0.1 for the 1996 AVIRIS data. For Hyperion, low SNR in the SWIR led to the use of only the 0.750 and 0.865 μm bands for the determination of the aerosol properties, and τ_{550} = 0.2 was derived for the

Hyperion data. However, because of the different season, the different time of day, there may be different sediment loads, different phytoplankton populations, and so perhaps somewhat different inherent optical properties (absorption and scattering profiles) in the water. To top it off, the intersection of the imagery has no deep water pixels (pixels that are unaffected by the reflectance of the ocean bottom) which would be in many ways the best to compare. We are left with comparisons of various locations in the image where the bottom is visible. Some results are shown in Figs. 2 & 3. In both cases, we have achieved reasonable (remarkable?) matches for $\lambda > 0.6$ µm. Is this merely fortuitous? As stated earlier, the tidal state is not going to be a great effect because the tides are so small, and yet the increasing absorption of light by water for $\lambda > 0.6$ µm (and therefore high sensitivity to depth in this wavelength range) would seem to indicate that the depths and bottom albedo are nearly identical when viewed 6.5 years apart. In both cases we have truncated the Hyperion spectra at about 0.43 µm, but truncation of Hyperion spectra at ~0.45 µm is not uncommon for ocean researchers, and is justified based on the noisiness in the bands at about 0.43 and 0.44 µm (Jupp, 2002). The atmospherically corrected Hyperion spectra all appear to be somewhat low in the blue compared to the atmospherically corrected AVIRIS spectra; however, even the atmospherically corrected AVIRIS spectra appear to be somewhat low at $\lambda < 0.45$ µm. While these results are tantalizing, a more thorough comparison still needs to be performed. This will require geocorrecting each image, or warping one of the images to the other, as well as resampling to a common spatial scale.

6. Conclusions

We have shown that it is possible to derive very similar spectra over shallow coastal areas from different hyperspectral sensor flown on different platforms, in different seasons, with different solar and view geometry. The derived atmospheric correction parameters for the two images using Tafkaa also differ. While there may be some calibration issues in the blue with both AVIRIS and Hyperion, the derived results are generally acceptable. Remote sensing of oceans with narrow field of view hyperspectral imagers in sun-synchronous orbits with off-nadir pointing ability allows us to avoid regions of high specular reflection. Such a sensor with high SNR in the VNIR and SWIR would allow derivation of aerosol parameters using the longer wavelengths and would be an ideal instrument for environmental assessment of the global coastal ocean.

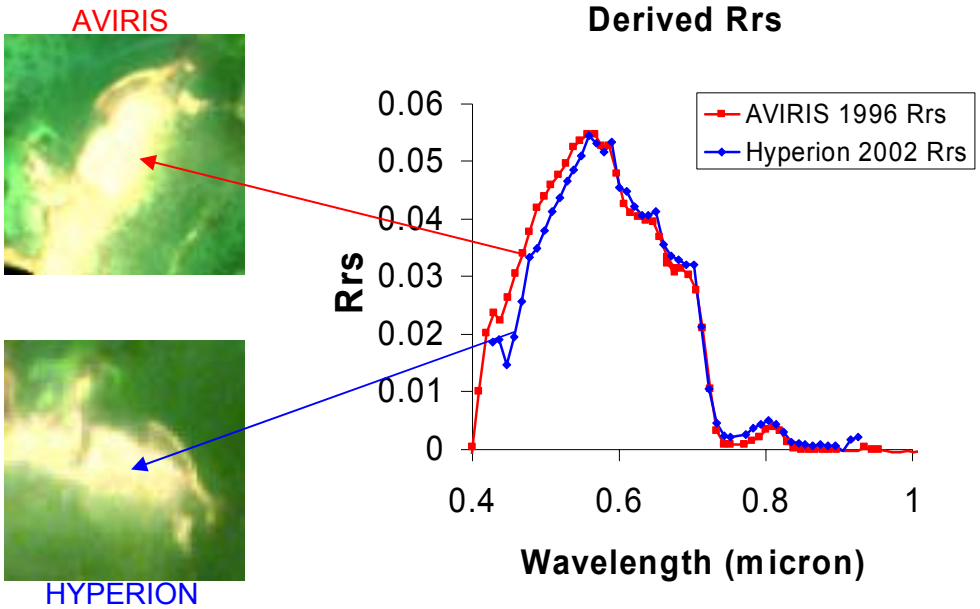

Figure 2. Spectra from a sandy region in the overlapping area; the images to the left are not georectified, but identification of identical features is obvious. The AVIRIS spectra are 3x3 pixel averages, and the Hyperion spectra are 2x2 pixel averages, in order to cover more similar spatial areas. The bump near 0.810 µm indicates a depth of < 2m.

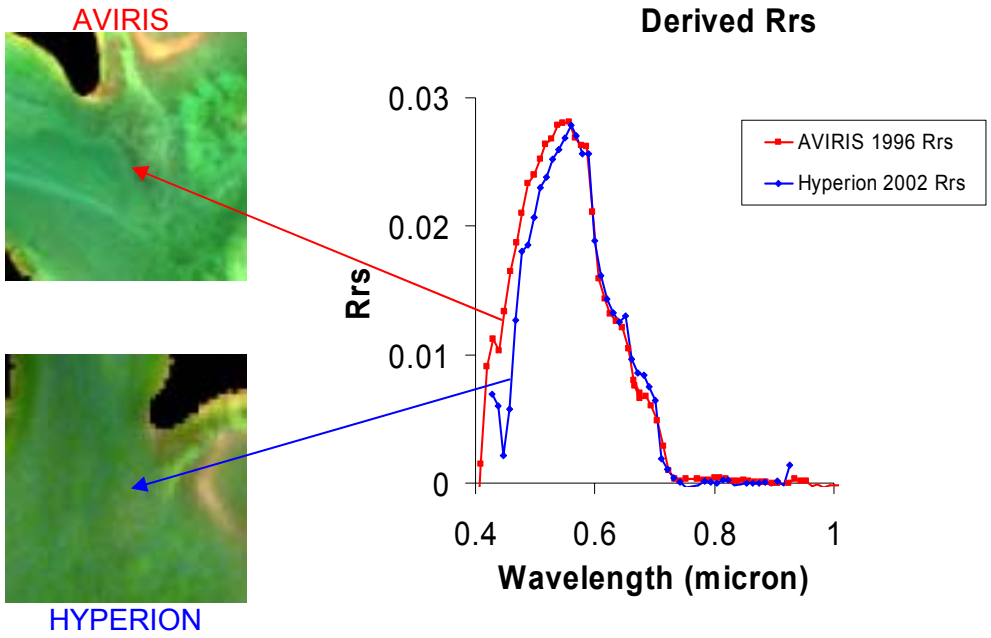

Figure 3. Same as in Figure 2, but from a deeper location and a different bottom type.

Acknowledgements

M. Montes, B.-C. Gao, and C. O. Davis received support from NASA and the Office of Naval Research.

References

Ahmad, Z. and R. S. Fraser, 1982, "An iterative radiative transfer code for ocean-atmosphere systems," *J. Atmos. Sci.*, 39, 656–665.

Cox, C., and W. Munk, 1954, "Statistics of the sea surface derived from sun glitter," *J. Mar. Res.*, 14, 63–78.

Datt, B., T. R. McVicar, T. G. Van Niel, D. L. B. Jupp, and J. S. Pearlman, 2003, "Preprocessing EO-1 Hyperion Hyperspectral Data to Support the Application of Agricultural Indices," *IEEE Trans. On Geosci. Rem. Sens.*, 41(6), 1246–1259.

Brando, V. E. and A. G. Dekker, 2003, "Satellite Hyperspectral Remote Sensing for Estimating Estuarine and Coastal Water Quality," *IEEE Trans. on Geosci. Rem. Sens.*, 41(6), 1378–1387.

Fraser, R. S., S. Matoo, E.-N. Yeh, and C. R. McClain, 1997, "Algorithm for atmospheric and glint corrections of satellite measurements," *J. Geophys. Res.*, 102, 17107–17118.

Gao, B.-C., M. J. Montes, Z. Ahmad, and C. O. Davis, 2000, "Atmospheric correction algorithm for hyperspectral remote sensing of ocean color from space," *Applied Optics*, 39(6), 887–896.

Goodenough, D. G., A. Dyk, K. O. Niemann, J. S. Pealman, H. Chen, T. Han, M. Murdoch, and C. West, 2003, "Preprocessing Hyperion and ALI for Forest Classification," *IEEE Trans. On Geosci. Rem. Sens.*, 41(6), 1321–1331.

Gordon, H. R., 1978, "Removal of atmospheric effects from satellite imagery of the oceans," *Appl. Opt.*, 17, 1631–1636.

Gordon, H. R., 1997, "Atmospheric correction of ocean color imagery in the Earth Observing System era," *J. Geophys. Res.*, 102, 17081–17106.

Gordon, H. R. and M. Wang, 1994, "Retrieval of water leaving radiance and aerosol optical thickness over the oceans with SeaWiFS: A preliminary algorithm," *Appl. Opt.*, 33, 443–452.

Green, R. O., B. E. Pavri, and T. G. Chrien, 2003, "On-Orbit Radiometric and Spectral Calibration Characteristics of EO-1 Hyperion Derived with an Underflight of AVIRIS and *In Situ* Measurements at Salar de Arizaro, Argentina," *IEEE Trans. On Geosci. Rem. Sens.*, 41(6), 1194–1203.

Jupp, D. L. B., 2002, "Discussion around Hyperion Data: Background notes for the Hyperion Data Users Workshop," CSIRO EOC, Canberra, Australia.

Kruse, F. A., J. W. Boardman, and J. F. Huntington, 2003, "Comparison of Airborne Hyperspectral Data and EO-1 Hyperion for Mineral Mapping," *IEEE Trans. on Geosci. Rem. Sens.*, 41(6), 1388–1400.

Montes, M. J., B.-C. Gao, and C. O. Davis, 2003, "Tafkaa atmospheric correction of hyperspectral data," in Proc. SPIE Vol. 5159 *Imaging Spectrometry IX*, S. S. Shen, P. E. Lewis, eds., (SPIE, Bellingham, Washington) pp. 188–197.

Montes, M. J., 2004, "AVIRIS Artifacts Appearing in Low-Light Imagery," *Proceedings of the 13th Airborne Earth Science Workshop,* this volume.

Special Issue on the Earth Observing (EO-1) Mission, IEEE Trans. On Geosci. Rem. Sens., 41(6), pp. 1147–1414, June 2003.